IEEE Access
Multidisciplinary | Rapid Review | Open Access Journal

Received July 18, 2020, accepted July 27, 2020, date of publication August 3, 2020, date of current version August 17, 2020.

Digital Object Identifier 10.1109/ACCESS.2020.3013835

Joint User Grouping and Decoding Order in Uplink/Downlink MISO/SIMO-NOMA

DINH-THUAN DO[1], (Senior Member, IEEE), THANH-LUAN NGUYEN[2], SABIT EKIN[3], (Member, IEEE), ZEESHAN KALEEM[4], AND MIROSLAV VOZNAK[5], (Senior Member, IEEE)

[1]Wireless Communications Research Group, Faculty of Electrical & Electronics Engineering, Ton Duc Thang University, Ho Chi Minh City 700000, Vietnam
[2]Faculty of Electronics Technology, Industrial University of Ho Chi Minh City (IUH), Ho Chi Minh City 700000, Vietnam
[3]School of Electrical and Computer Engineering, Oklahoma State University, Stillwater, OK 74078, USA
[4]Department of Electrical and Computer Engineering, COMSATS University Islamabad, Wah Campus, Wah 47040, Pakistan
[5]Faculty of Electrical Engineering and Computer Science, Technical University of Ostrava, 70833 Ostrava, Czech Republic

Corresponding author: Dinh-Thuan Do (dodinhthuan@tdtu.edu.vn)

This work was supported by the Czech Ministry of Education, Youth and Sports through the VSB - Technical University of Ostrava under Grant SP2020/65.

ABSTRACT In this paper, we design and investigate a novel uplink/downlink (UL/DL) non-orthogonal multiple access (NOMA) network using a common relay. Instead of successive interference cancellation (SIC) for UL/DL NOMA systems with fixed decoding order based on the statistical channel state information (CSI), we adopt the dynamic decoding order according to power level of received signals. Specifically, by exploiting the CSI-based dynamic decoding order, better fairness can be achieved and applicable. This decoding scheme is highly suitable for implementing a NOMA system in practice. The closed-form expressions for the users' outage probabilities are derived, and then an asymptotic analysis is carried out. Insightful discussions with diversity order are provided. Simulations are performed to corroborate the exactness of the theoretical analysis.

INDEX TERMS Uplink/downlink, non-orthogonal multiple access, outage probability, dynamic decoding order.

I. INTRODUCTION

A new radio access technology (RAT) approach is actively pursued and studied to meet demands including very high-speed data rates and massive connections in the next generation (5G) cellular network. As a promising candidate for RAT, non-orthogonal multiple access (NOMA) is recommended to widely implement in 5G wireless system [1]. In contrast to orthogonal multiple access (OMA), multiple NOMA users are able to share frequency/time resources at the same time and offer numerous benefits [2]. Recent studies have presented the advantages of NOMA scheme such as providing higher throughput for cell-edge users, improving spectral efficiency, enhancing connectivity and reducing transmission latency [3], [4]. In NOMA, superimposed signals are performed at transmitters while successive interference cancellation (SIC) is utilized at receivers to detect the superimposed messages which are assigned to different power allocation coefficients [5]–[8].

The associate editor coordinating the review of this manuscript and approving it for publication was Liqun Fu.

To overcome the challenges encompassing the next-generation wireless networks, power domain NOMA was extensively studied in emerging networks [9]–[16]. In particular, NOMA is considered an attractive technique due to the ability to serve multiple users in the same frequency, time, or code resource thus providing efficient access to massive connections [9], [11]. As compared to OMA, in NOMA, the machine types communication devices in Narrowband-Internet of Things (NB-IoT) are allocated to different ranks within the NOMA clusters and are allowed to transmit over the same frequency resources [15]. The authors in [16] explored joint subcarrier and power allocation problems in NB-IoT system for both transmission modes to provide maximum connection density while satisfying the Quality of Service (QoS) requirements and the transmit power constraints of IoT devices. Furthermore, to mitigate aerial-ground interference mitigation in the cellular-connected unmanned aerial vehicle (UAV) network, NOMA is applied under spectrum sharing feature with the existing ground users [17]. A hybrid satellite/unmanned

aerial vehicle (HSUAV) terrestrial NOMA network was studied to permit satellite to communicate with ground users with the assistance of UAV relay using a decode-forward (DF) protocol [18].

The authors in [19] studied the optimal power allocation for NOMA by considering several objective functions and constraints. A novel power allocation scheme and user pairing are studied to reduce the computational complexity in [20]. The authors in [21] presented the clustering and resource block allocation in multi-carrier uplink NOMA networks. Meanwhile, emerging transmission techniques, namely full-duplex communications, multiple-input multiple-output (MIMO) systems, and heterogeneous systems are considered in [9], [22], [23] to introduce advanced approaches associated with NOMA. To obtain benefits from both OMA and NOMA, a hybrid of OMA and NOMA in 5G has been explored in [24] and [25]. In [24], considering downlink (DL) of a NOMA-based cell-free massive MIMO system, the classic max-min optimization framework is studied for achieving the optimal minimum bandwidth efficiency of a user. In particular, in [24], an operating mode switching scheme is proposed where OMA/NOMA selection depends on two conditions including the total number of users and the length of the channel's coherence time. The authors in [25] considered a heterogeneous network in which OMA and NOMA coexist. In particular, they employed dynamic power assignment and four generic pairing schemes for NOMA including Hungarian, Gale-Shapley, random, and exhaustive.

A. RELATED WORKS

In [26], the impact of the decoding order implemented at the SIC receiver was studied for downlink (DL) NOMA systems. In [27], the ergodic sum capacity of uplink (UL) NOMA was computed in terms of imperfect and perfect SIC. Furthermore, the implementation of NOMA was extended to cooperative UL/DL relay schemes (referred to as relay sharing NOMA) in [28], [29], where an intermediate relay was deployed to assist two pairs of source-destination nodes. An extention of [28] is done by [30], in which the authors assume Nakagami-m fading with integer shapes. As well-known fundamentals, the difference in users' channel conditions is crucial for realizing the potential of NOMA [31]. However, users who possess similar channel conditions need different power allocation schemes to participate in NOMA. In [32], the authors examined the decoding order, user grouping and power control in an uplink NOMA system. They formulated a joint optimization problem to achieve the optimal sum rate of multiple users. In addition, the dynamic decoding order and power allocation of received signals are difficult to obtain for UL/DL NOMA when the fairness requirement is considered, which is still an open issue.

Moreover, to further enhance the performance of the SIC receiver in NOMA networks, the authors in [33], [34] proposed a dynamic decoding order scheme which exploits the disparity in the channel gain among uplink users. Later on, this optimal ordering is then further examined in [35]–[37]. In [35], the authors propose approximation for the uplink multiuser NOMA enabling dynamic decoding order via shifted-gamma distribution. Moreover, the work in [36] compares the conventional fixed decoding order with the dynamic one. An advanced SIC receiver that orders the uplink users based on their statistical channel state information is introduced in [37]. However, the above works are limited to Rayleigh fading channels.

In the literature, the Nakagami-m fading is a better model than Rayleigh fading due to its capability in modeling a wider range of wireless channels, where it can even capture the Rayleigh fading when the fading order, i.e., the shape factor, equals one ($m = 1$) [38]. Furthermore, the study in [39] shows that the Nakagami-m model can provide highly accurate empirical data for much more complex fading which is the $\kappa - \mu$ shadowed fading. In particular, the $\kappa - \mu$ shadowed fading is the generalized model for many fading models such as Rician shadowed, Ricican-K, $\eta-\mu$, $\kappa-\mu$, and have important applications in the hybrid satellite-terrestrial communication as well as the underwater acoustic communications [40].

B. CONTRIBUTION

To the best of our knowledge, among the existing works on UL/DL NOMA scheme, in Nakagami-m fading environment with the dynamic decoding order has not been studied. It is assumed that the intermediate node (relay) is able to achieve full knowledge of the CSI of all users and SIC can eliminate interference. Besides, to perform the signal detection successfully, the need to know the conditions of channels. The main contributions can be concluded as follows.

- Different from the the related work in literature such as [5], [32], group of transmitter/receiver relying on NOMA and dynamic power allocation scheme are adopted in this paper. The fairness among two users depends on the received power at users. Designs of multiple input single output (MISO) and single input multiple output (SIMO) are adopted in such NOMA network [41].
- Unlike [28], [29], where Rayleigh fading model is adopted, we take the Nakagami-m fading model into consideration. The exact analytical expressions for the outage probability at each destination are derived under real-valued fading orders. In addition, the derived results can be utilized to extend results reported in [30].
- To further evaluate system performance, analysis in the high transmit power regime, i.e., asymptotic analysis and diversity order, are provided for additional insights.
- Under UL/DL NOMA with dynamic decoding order, we observe multiple cases for the diversity order at each destination, in which there are only four cases for non-zero diversity order.

The rest of this paper is organized as follows. Section II presents the system model, the signal decoding order, the signal-to-interference-plus-noise ratio (SINR) and the

signal-to-noise ratio (SNR) of the UL/DL transmissions. Section III describes the outage probability in UL and DL. Then, we provide analytical preliminaries, exact expressions, asymptotic and diversity order at the destinations. Section IV further provides the numerical results to validate the analysis in the previous sections and describes main parameters affecting on the performances of the UL/DL NOMA system. Finally, Section V concludes this paper.

Notation: Vectors are symbolized by bold-faced letters, e.g., $\mathbf{x}$, $\|\bullet\|_F$ specifies the Frobenius norm, $(\bullet)^T$ and $(\bullet)^H$ denote the normal and Hermitian transpose, respectively. Moreover, $\mathcal{CN}(0, \Omega)$ denotes the complex circular Gaussian random variable (RV) with zero mean and variance Ω and $\mathcal{G}(\alpha, \beta)$ denotes the Gamma distributed RV with parameters, i.e. α and β.

II. SYSTEM MODEL

This paper studies a cooperative relay sharing network consisting a M_1-antenna source S_1 and a M_2-antenna source S_2 intend to simultaneously transmits their unit energy symbols, namely x_1 and x_2, to the K_1-antenna destination D_1 and the K_2-antenna destination D_2, respectively, as shown in the Fig. 1. Assuming that heavy shadowing and multiple blockage present at the direct $S_1 - D_1$ and $S_2 - D_2$ links, and hence a DF-based relay R is selected to assist the transmission between each $S_n - D_n$ pair ($n = 1, 2$). The complex channels between of the $S_n - R$ link are denoted by $\mathbf{g}_n = [g_{n,1}, \ldots, g_{n,M_n}] \in \mathbb{C}^{1\times M_n}$ and that of the $R - D_n$ link is $\mathbf{h}_n = [h_{n,1}, \ldots, h_{n,K_n}]^T \in \mathbb{C}^{K_n\times 1}$. In this paper, the fading amplitudes $|g_{n,m}|$ and $|h_{n,k}|$ is modeled as Nakagami-m distributed RVs with severity factors $m_n > 0.5$ and $k_n > 0.5$, respectively, and unit variances $\forall m \in [1, M_n]$ and $k \in [1, K_n]$. We assume that all available channels are independent. In addition, power-law path-loss model is also applied for evaluating the system performance where $\alpha (2 \le \alpha < 7)$ denotes the path-loss exponent.

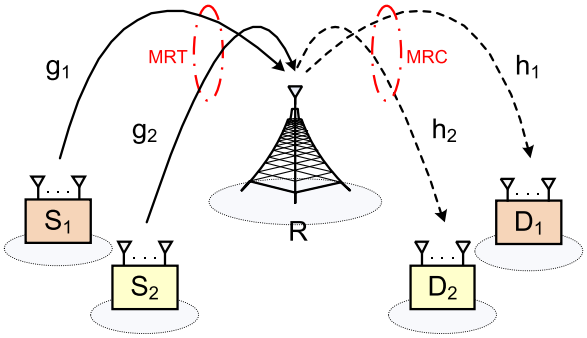

FIGURE 1. The proposed uplink/downlink MISO/SIMO-NOMA.

The transmission from the sources to the corresponding destinations can be considered as two operations including the uplink transmission in the first phase and the downlink transmission in the second phase. Unlike [28], [29], where the uplink/downlink channel quality is dominant by their distances to the relay due to the assumption of Rayleigh fading, the quality of Nakagami-m channels are not only determined by the distances but also by the fading severity. As a general case, the Nakagami-m model can be utilized to approximate Rician-K fading where the line-of-sight (LoS) components exist as well as can model the Rayleigh channels when all the shapes equal ones.

The cooperative transmission, which is divided via two phases, in the proposed model is described as follows.

A. UPLINK TRANSMISSION

During this phase, the sources S_1 and S_2 simultaneously transmit the normalized information signal x_1 and x_2, respectively, to the relay. Assuming perfect time synchronization between both sources, [43], [44], the received signal at the relay R is written as

$$y_R = \frac{\sqrt{P_1}}{\sqrt{d_1^\alpha}}\mathbf{g}_1\mathbf{m}_1 x_1 + \frac{\sqrt{P_2}}{\sqrt{d_2^\alpha}}\mathbf{g}_2\mathbf{m}_2 x_2 + n_R, \tag{1}$$

in which P_n specifies the transmit powers, d_n denotes the distance of the $S_n - R$ link, $n_R \sim \mathcal{CN}(0, \sigma_R^2)$ is the additive white Gaussian noise (AWGN) observed at the relay and $\mathbf{m}_n \in \mathbb{C}^{M_n\times 1}$ specifies the transmit beamforming vector at the n-th source node. It is asserted that the term $P_n d_n^{-\alpha} |\mathbf{g}_n\mathbf{m}_n|^2$ denote the power of the received signal x_n.

For simplicity and tractability purposes, the Maximum Ratio Transmission (MRT) linear processing adopted at each source S_n, and thus the beamforming vectors are designed as [45], [46]

$$\mathbf{m}_n = \frac{(\mathbf{g}_n^T)^H}{\|\mathbf{g}_n^T\|_F}, \quad n = 1, 2. \tag{2}$$

Consequently, the power of the received signal x_n from the corresponding source becomes $P_n d_n^{-\alpha} \|\mathbf{g}_n\|_F^2$. By employing SIC, the relay decodes the message with higher received power first then decodes the lower one after perfectly canceling the previously detected signal [27]. In other words, the decoding at the relay in the uplink phase can be viewed separately via two scenarios

- Scenario-1: The power of the received signal x_1 is higher than that of the signal x_2.
- Scenario-2: The power of the received signal x_2 is higher than that of the signal x_1.

In the first scenario, i.e., $P_1\, d_1^{-\alpha}\, \|\mathbf{g}_1\|_F^2 > P_2\, d_2^{-\alpha}\, \|\mathbf{g}_2\|_F^2$, the received signal-to-interference-plus-noise ratios (SINR) at the relay R to decode x_1 and x_2 successively are

$$\gamma_{1\to 2} = \frac{\frac{P_1}{d_1^\alpha}\|\mathbf{g}_1\|_F^2}{\frac{P_2}{d_2^\alpha}\|\mathbf{g}_2\|_F^2 + \sigma_R^2} \text{ and } \gamma_2 = \frac{\frac{P_2}{d_2^\alpha}\|\mathbf{g}_2\|_F^2}{\sigma_R^2}, \tag{3}$$

respectively.

In the second scenario, i.e., $P_2\, d_2^{-\alpha}\, \|\mathbf{g}_2\|_F^2 > P_1\, d_1^{-\alpha}\, \|\mathbf{g}_1\|_F^2$, the received instantaneous SINRs to decode x_2 and x_1 in a successive manner are given by

$$\gamma_{2\to 1} = \frac{\frac{P_2}{d_2^\alpha}\|\mathbf{g}_2\|_F^2}{\frac{P_1}{d_1^\alpha}\|\mathbf{g}_1\|_F^2 + \sigma_R^2} \text{ and } \gamma_1 = \frac{\frac{P_1}{d_1^\alpha}\|\mathbf{g}_1\|_F^2}{\sigma_R^2}, \tag{4}$$

respectively.

Remark 1: Comparing to the fixed-order decoding scheme in many papers, e.g., [8], [10], [31], the dynamic-order decoding scheme also exploits channel estimators for coherent detection. Hence, the signaling overhead incurred by both schemes is due to the estimation and sorting of the received signal strength. Although the dynamic-order approach requires an the deployment of an additional order determination block, the complexity and latency are quite similar to the fixed-order decoder.

B. DOWNLINK TRANSMISSION

In this phase, after x_1 and x_2 being correctly recovered, the relay mixes the decoded signals by the use of superposition coding, forming $x_R = \sqrt{\rho_1}x_1 + \sqrt{\rho_2}x_2$, in which $\rho_n \in (0, 1)$ specifies the fraction of power allocated for the decoded signal x_n and $\rho_1 + \rho_2 = 1$. The superimposed mixture x_R is then broadcasted to both destinations. Accordingly, the received signal at each n-th destination can be formulated by

$$y_n = \frac{\sqrt{P_R}}{\sqrt{l_n^{\alpha}}}\mathbf{k}_n^H \mathbf{h}_n x_R + w_n, \tag{5}$$

in which P_R is the transmit power, $w_n \sim \mathcal{CN}(0, \sigma_n^2)$ denotes the AWGN at the node D_n and $\mathbf{k}_n \in \mathbb{C}^{K_n \times 1}$ is the receive beamforming vector at the D_n.

By employing maximum ratio combining (MRC) scheme, each destination D_n employs the normalized vector $\mathbf{k}_n$ as [46]

$$\mathbf{k}_n = \frac{\mathbf{h}_n^H}{\|\mathbf{h}_n\|_F}. \tag{6}$$

Moreover, to guarantee the fairness in the performance at the DL nodes, the relay should allocate more power for the destination with worse channel condition and vice versa, which in turns decides the decoding order each D_n. Particularly, the dynamic-order decoding at both DL nodes can be viewed separately via two scenarios

- Scenario-1: The weighted channel gain at D_1 is higher than that at D_2.
- Scenario-2: The weighted channel gain at D_2 is higher than that at D_1.

In the first scenario, i.e., $l_1^{-\alpha}\|\mathbf{h}_1\|_F^2 > l_2^{-\alpha}\|\mathbf{h}_2\|_F^2$, the relay then allocates more power for the node D_2, i.e., $\rho_1 < \rho_2$. Therefore, the destination D_1 needs to perform SIC to cancel x_2 before detecting x_1 whereas D_2 can directly decode x_2. Accordingly, the instantaneous SINRs at the D_1 before, after SIC are given as

$$\gamma'_{2\to 1} = \frac{\rho_2 \frac{P_R}{l_1^{\alpha}}\|\mathbf{h}_1\|_F^2}{\rho_1 \frac{P_R}{l_1^{\alpha}}\|\mathbf{h}_1\|_F^2 + \sigma_n^2}, \ \gamma'_1 = \frac{\rho_1 \frac{P_R}{l_1^{\alpha}}\|\mathbf{h}_1\|_F^2}{\sigma_n^2}, \tag{7}$$

respectively. Meanwhile, the instantaneous SINR observed at the D_2 is

$$\gamma'_{2/1} = \frac{\rho_2 \frac{P_R}{l_2^{\alpha}}\|\mathbf{h}_2\|_F^2}{\rho_1 \frac{P_R}{l_2^{\alpha}}\|\mathbf{h}_2\|_F^2 + \sigma_n^2}. \tag{8}$$

In the second scenario, i.e., $l_2^{-\alpha}\|\mathbf{h}_2\|_F^2 > l_1^{-\alpha}\|\mathbf{h}_1\|_F^2$, the relay allocates more power for D_1, thus the user D_2 needs to perform SIC to cancel x_1 before detecting x_2, whereas D_1 can directly decode x_1. Accordingly, the instantaneous SINRs at D_2 before, after SIC are given as

$$\gamma'_{1\to 2} = \frac{\rho_1 \frac{P_R}{l_2^{\alpha}}\|\mathbf{h}_2\|_F^2}{\rho_2 \frac{P_R}{l_2^{\alpha}}\|\mathbf{h}_2\|_F^2 + \sigma_n^2}, \ \gamma'_2 = \frac{\rho_2 \frac{P_R}{l_2^{\alpha}}\|\mathbf{h}_2\|_F^2}{\sigma_n^2}, \tag{9}$$

respectively. Meanwhile, the instantaneous SINR observed at the D_1 is

$$\gamma'_{1/2} = \frac{\rho_1 \frac{P_R}{l_1^{\alpha}}\|\mathbf{h}_1\|_F^2}{\rho_2 \frac{P_R}{l_1^{\alpha}}\|\mathbf{h}_1\|_F^2 + \sigma_n^2}. \tag{10}$$

III. OUTAGE PERFORMANCE ANALYSIS

This section studies the outage performance at each D_n under optimal decoding order strategies. To grasp the concept of outage probability, let us define $\tau_n \triangleq 2^{2\bar{R}_n} - 1$ (dB) as the decoding threshold of x_n, in which $\bar{R}_n$ (bps/Hz) denotes the corresponding data rate.

In the UL, the outage event occurs whenever the instantaneous SINR to decode any x_n drops below τ_n or, in other words, the relay cannot decode both x_1 and x_2. Regarding the determined decoding order, the outage probability at the relay can be formulated by

$$\begin{aligned} P_R^{out} &= 1 - \Pr\{\gamma_{1\to 2} > \tau_1, \gamma_2 > \tau_2, \phi_1 > \phi_2\} \\ &\quad - \Pr\{\gamma_{2\to 1} > \tau_2, \gamma_1 > \tau_1, \phi_2 > \phi_1\}, \end{aligned} \tag{11}$$

in which $\phi_n \triangleq \bar{P}_n d_n^{-\alpha}\|\mathbf{g}_n\|_F^2$ and $\bar{P}_n \triangleq P_n/\sigma_R^2$.

Remark 2: From (11)*, it can be perceived that when the occurring probability of the event $\phi_1 > \phi_2$ or $\phi_1 < \phi_2$ reaches one, the dynamic (optimal) decoding order can have similar performance as the fixed decoding order. Further, the fixed decoding order requires significant channel disparities between the uplink users and thus become impotent when their channel conditions are similar. In addition, when considering a scenario where one user has LoS but it is located far from the BS and the other user has no LoS (nLoS) but it is located closer, the model in [28], [29] cannot correctly evaluate the system performance.*

In the DL, the outage probability at the n-th destination can be written in an unified-form as

$$\begin{aligned} P_{R\to D_n}^{out} &= 1 - \Pr\{\gamma'_{n/t} \geq \tau_n, \psi_n < \psi_t\} \\ &\quad - \Pr\{\gamma'_{t\to n} \geq \tau_t, \gamma'_n \geq \tau_n, \psi_n > \psi_t\}, \end{aligned} \tag{12}$$

in which $\psi_n \triangleq \bar{P}_R l_n^{-\alpha}\|\mathbf{h}_n\|_F^2$ and $\bar{P}_R \triangleq P_R/\sigma_n^2$. From this point till the rest of the paper, we use $(n, t) = (1, 2), (2, 1)$.

Therefore, the outage probability at the D_n can be formulated by

$$P_{D_n}^{out} = 1 - (1 - P_R^{out})(1 - P_{R\to D_n}^{out}). \tag{13}$$

In the next subsection, we provide some preliminary results to assist the upcoming analysis of the proposed system.

A. PRELIMINARY

To support the analysis of P_R^{out} in the upcoming sections, we introduce the following probabilities

$$Q(\phi_n, \phi_t; z) = \Pr\{\phi_n > \phi_t, \phi_t > z\}, \quad (14)$$

$$P(\phi_n, \phi_t; y, z) = \Pr\{\phi_n > y(\phi_t + 1), \phi_t > z\}. \quad (15)$$

It is recalled that $|g_{n,m}|, \forall m \in [1, M_n]$, follows Nakagami distribution, thus the power gain $|g_{n,m}|^2$ can be modeled by Gamma distribution with shape m_n and unit mean. By definition, $\|\mathbf{g}_n\|_F^2 = \sum_{m=1}^{M_n} |g_{n,m}|^2$, thus $\phi_n \triangleq \bar{P}_n d_n^{-\alpha} \|\mathbf{g}_n\|_F^2$ can be viewed as the sum of M_n i.i.d. Gamma distributed RVs and thus can be modeled as $\phi_n \sim \mathcal{G}(M_n m_n, \mu_n/m_n)$ in which $\mu_n \triangleq \bar{P}_n d_n^{-\alpha}$. Subsequently, the PDF and CDF of the defined ϕ_n can be expressed as

$$f_{\phi_n}(\phi) = \frac{(\frac{m_n}{\mu_n})^{M_n m_n}}{\Gamma(M_n m_n)} \phi^{M_n m_n - 1} e^{-\frac{m_n \phi}{\mu_n}}, \quad \phi > 0, \quad (16)$$

$$F_{\phi_n}(\phi) = \frac{1}{\Gamma(M_n m_n)} \gamma\left(M_n m_n; \frac{\phi m_n}{\mu_n}\right), \quad \phi > 0, \quad (17)$$

respectively, in which $\gamma(m; \mu) = \int_0^{\mu} x^{m-1} e^{-x} \mathrm{d}x$ is the lower incomplete Gamma function [47, 8.35] and $\Gamma(x) = \int_0^{\infty} t^{x-1} e^{-t} \mathrm{d}t$ denotes the Gamma function.

Accordingly, the closed-form of the probability $Q(\phi_n, \phi_t; z)$ with arbitrary m_1 and m_2 can be derived by the following proposition.

Proposition 1: For arbitrary parameters m_1 and m_2, the defined probability $Q(\phi_n, \phi_t; z)$ in (14) can be expressed as

$$Q(\phi_n, \phi_t; z) = Q(\phi_n, \phi_t; 0) - F_{\phi_t}(z) + \Delta(\phi_n, \phi_t; z), \quad (18)$$

in which $Q(\phi_n, \phi_t; 0)$ is provided by (19), as shown at the bottom of the page, where ${}_2F_1(a_1, a_2; b; z)$ denotes the Gaussian hypergeometric function [47, 9.1], $\mathbf{B}(a; b) = \frac{\Gamma(a+b)}{\Gamma(a)\Gamma(b)}$ is the Beta function, and

$$\Delta(\phi_n, \phi_t; z) = \sum_{l=1}^{L} \zeta_l f_{\phi_t}(t_l) F_{\phi_n}(t_l), \quad (20)$$

in which $\zeta_l \triangleq \frac{z\pi}{2L}\sqrt{1-\delta_l^2}$, $\delta_l \triangleq \cos(\frac{2l-1}{2L}\pi)$, $t_l \triangleq \frac{z}{2}(1+\delta_l)$ and L represents the accuracy of the Gaussian-Chebyshev quadratute [49].

Proof: See Appendix V. ∎

Moreover, the defined probabilities $P(\phi_n, \phi_t; y, z)$ in (16) can be derived as

$$P(\phi_n, \phi_t; y, z) = \frac{(\frac{m_t}{\mu_t})^{M_t m_t}}{\Gamma(M_n m_n)\Gamma(M_t m_t)} \times \int_z^{\infty} t^{M_t m_t - 1} e^{-\frac{m_t t}{\mu_t}} \Gamma\left(M_n m_n; \frac{m_n}{\mu_n}(t+1)y\right) \mathrm{d}t, \quad (21)$$

in which $\Gamma(m; \mu) = \int_{\mu}^{\infty} x^{m-1} e^{-\mu} \mathrm{d}x$ specifies the upper incomplete Gamma function [47, 8.35]. In general, the above integral has no tractable closed-form with arbitrary m_n and m_t. However, when both m_n and m_t are integer values, the closed-form for the above integral can be obtained by the following corollary.

Corollary 1: Assuming that both m_1 and m_2 are integers, the integral $P(\phi_n, \phi_t; y, z)$ in (21) can be derived as

$$P(\phi_n, \phi_t; y, z) = \frac{1}{\Gamma(M_t m_t)} \exp\left(-\frac{m_n y}{\mu_n}\right) \left(\frac{m_t}{\mu_t}\right)^{M_t m_t} \times \sum_{m=0}^{M_n m_n - 1} \frac{1}{m!} \left(\frac{m_n y}{\mu_n}\right)^m \sum_{k=0}^{m} \binom{m}{k} \left(\frac{m_t}{\mu_t} + \frac{m_n y}{\mu_n}\right)^{-m_t - k} \times \Gamma\left(M_t m_t + k; \left(\frac{m_n y}{\mu_n} + \frac{m_t}{\mu_t}\right) z\right). \quad (22)$$

Proof: By applying the identity [47, Eq. (8.352.4)] for the incomplete Gamma function as $\frac{\Gamma(n,x)}{\Gamma(n)} = e^{-x} \sum_{k=0}^{n-1} \frac{x^k}{k!}$, the integral $P(\phi_n, \phi_t; y, z)$ in (21) can be further derived as

$$P(\phi_n, \phi_t; y, z) = \frac{1}{\Gamma(M_t m_t)} \exp\left(-\frac{m_n y}{\mu_n}\right) \left(\frac{m_t}{\mu_t}\right)^{M_t m_t} \times \sum_{m=0}^{M_n m_n - 1} \frac{1}{m!} \left(\frac{m_n y}{\mu_n}\right)^m \int_z^{\infty} x^{M_t m_t - 1} (x+1)^m \times \exp\left(-\left(\frac{m_t}{\mu_t} + \frac{m_n y}{\mu_n}\right) x\right) \mathrm{d}x. \quad (23)$$

Following the binomial theorem $(x+1)^m = \sum_{k=0}^{m} \binom{m}{k} x^k$ and then applying [47, Eq. (3.381.3)], we then obtain the result. ∎

To shed more light on the analysis of $P(\phi_n, \phi_t; y, z)$ with arbitrary parameters, we consider the following Taylor series at the expansion point z_0 given by

$$\Gamma(v; z) = \Gamma(v; z_0) - z_0^v e^{-z_0} \sum_{i=1}^{\infty} \sum_{j=0}^{i-1} \eta(v; i, j) \frac{(z - z_0)^i}{(z_0)^{i-j}}, \quad (24)$$

in which $\eta(v; i, j) \triangleq \frac{1}{i} \frac{(-1)^j}{j!} \frac{(v-i+j+1)_{i-j-1}}{(i-j-1)!}$ with $(x)_y$ being the Pochhammer symbol.

Proof: See Appendix V. ∎

The idea is to rewrite the upper incomplete Gamma term in (21) as the infinite sum of simpler functions using series expansion. The common approach is to apply the familiar Mclaurin series $\Gamma(a; z) = \Gamma(a) - \sum_{i=0}^{I=\infty} \frac{(-1)^i z^{a+i}}{i!(a+i)}$ [47, Eq. (8.354.2)], where the truncated version ($I < \infty$) often provides good approximation for $\Gamma(a; z)$ at the point

$$Q(\phi_n, \phi_t; 0) = \frac{{}_2F_1\left(M_t m_t, M_t m_t + M_n m_n; M_t m_t + 1; -\frac{m_t \mu_n}{m_n \mu_t}\right) \left(\frac{m_t \mu_n}{m_n \mu_t}\right)^{M_t m_t}}{M_t m_t \mathbf{B}(M_t m_t; M_n m_n)} \quad (19)$$

$z_0 = 0$. However, our main goal is to later analyze the probability $P(\phi_n, \phi_t; y, z)$ in the high transmit power regime, where the term "$\frac{m_n(t+1)y}{\mu_n}$" in (21) tends to reach "$z_0 = \frac{m_n y t}{\mu_n}$" instead of zero. Thus, applying the proposed series in (24) can result a better approximation with lower complexity.

Specifically, based on the given Taylor series, we then deal with the integral in (21) via the following proposition.

Proposition 2: Under arbitrary m_1 and m_2, the probability $P(\phi_n, \phi_t; y, z)$ can be expressed via the infinite series in (25)*, as shown at the bottom of the page.*

Proof: Applying (25) at the expansion point $z_0 = \frac{m_n y}{\mu_n} t$ into (22) and then using [47, Eq. (3.381.3)] we can obtain the desired result. ■

B. ANALYTICAL RESULTS

In this subsection, we provide the analytical expressions for the outage probabilities at the relay and the destinations.

1) UPLINK TRANSMISSION

The analytical expression of the outage probability at the relay is presented in the following proposition. It is notable that the given result is expressed in terms of the previous probabilities, and later can be adopted for asymptotic analysis.

Proposition 3: With the aid of the self-defined probabilities $Q(\phi_n, \phi_t; z)$ in (14) *and $P(\phi_n, \phi_t; y, z)$ in* (15)*, the outage probability at the relay is given as*

$$P_R^{out} = 1 - P(\phi_1, \phi_2; \tau_1, \tau_2) - P(\phi_2, \phi_1; \tau_2, \tau_1) - \begin{cases} Q(\phi_1, \phi_2; \theta_2) - P(\phi_1, \phi_2; \tau_1, \theta_2), & \tau_1 < 1 \\ 0, & \tau_1 \geq 1 \end{cases} - \begin{cases} Q(\phi_2, \phi_1; \theta_1) - P(\phi_2, \phi_1; \tau_2, \theta_1), & \tau_2 < 1 \\ 0, & \tau_2 \geq 1 \end{cases} \tag{26}$$

in which $\theta_1 = \max\left(\tau_1, \frac{\tau_2}{1-\tau_2}\right)$ and $\theta_2 = \max\left(\tau_2, \frac{\tau_1}{1-\tau_1}\right)$.

Proof: See Appendix V. ■

Remark 3: With x_1 being decoded first, the defined probability $P(\phi_1, \phi_2; \tau_1, \tau_2)$ can cover the analysis of the outage probability at the relay for the fixed-order decoder in [30]. Analogously, the term $P(\phi_2, \phi_1; \tau_2, \tau_1)$ can be used for the case where x_2 being decoded first.

2) DOWNLINK TRANSMISSION

To assist the analysis for the DL performance, let $\rho \triangleq \min(\rho_1, \rho_2)$ denote the power allocation for the stronger D_n. Hence, the outage probability at D_1 and D_2 in the DL can be expressed in an unified-form as

$$P_{R\to D_n}^{out} = 1 - \Pr\left\{\frac{(1-\rho)\psi_n}{\rho\psi_n + 1} > \tau_n, \psi_n < \psi_t\right\} - \Pr\left\{\frac{(1-\rho)\psi_n}{\rho\psi_n + 1} > \tau_t, \rho\psi_n > \tau_n, \psi_n > \psi_t\right\}. \tag{27}$$

With some simple steps, the above probability can be rewritten as

$$\begin{aligned} P_{R\to D_n}^{out} &= 1 - \Pr\left\{\psi_n > \vartheta_n, \psi_n < \psi_t \,\middle|\, \rho < (1+\tau_n)^{-1}\right\} - \Pr\left\{\psi_n > \vartheta_n', \psi_n > \psi_t \,\middle|\, \rho < (1+\tau_t)^{-1}\right\}, \\ &\triangleq 1 - (\Pr_1 + \Pr_2), \end{aligned} \tag{28}$$

where $\vartheta_n \triangleq \frac{\tau_n}{1-\rho(\tau_n+1)}$ and $\vartheta_n' \triangleq \max\left(\frac{\tau_n}{\rho}, \frac{\tau_t}{1-\rho(\tau_t+1)}\right)$.

The first probability in (28) ($\Pr_1$) can be derived as

$$\Pr_1 = Q(\psi_t, \psi_n; \vartheta_n) \tag{29}$$

with $\rho < (1+\tau_n)^{-1}$ whereas

$$\Pr_2 = 1 - F_{\psi_n}(\vartheta_n') - Q(\psi_t, \psi_n; \vartheta_n') \tag{30}$$

with $\rho < (1+\tau_t)^{-1}$, in which $F_{\psi_n}(\psi)$ is the CDF of ψ_n. Recalling that $\psi_n \triangleq \bar{P}_R l_n^{-\alpha} \|\mathbf{h}_n\|_F^2$, and thus ψ_n can also be viewed as the sum of i.i.d. Gamma distributed RVs. In other words, $\psi_n \sim \mathcal{G}(K_n k_n; \lambda_n/k_n)$ in which $\lambda_n \triangleq \bar{P}_R l_n^{-\alpha}$. Hence, its PDF and CDF can be obtained analogously to (14) and (15), respectively, in which $k_n \equiv m_n$, $K_n \equiv M_n$ and $\lambda_n \equiv \mu_n$.

Subsequently, the probability $P_{R\to D_n}^{out}$ given in (28) can be evaluated via $\Pr_1$ in (29) and $\Pr_2$ in (30).

Proposition 4: The probability $P_{R\to D_n}^{out}$ can be expressed in terms of $\Pr_1$ and $\Pr_2$ as

$$P_{R\to D_n}^{out} = 1 - \begin{cases} \Pr_1 + \Pr_2, & \rho < \rho_{\max} \\ \Pr_2, & \rho_{\max} \leq \rho < \rho_{\min}, \tau_n > \tau_t \\ \Pr_1, & \rho_{\max} \leq \rho < \rho_{\min}, \tau_n < \tau_t \\ 0, & \rho \geq \rho_{\min} \end{cases} \tag{31}$$

in which $\rho_{\max} \triangleq \frac{1}{1+\max(\tau_1,\tau_2)}$ and $\rho_{\min} \triangleq \frac{1}{1+\min(\tau_1,\tau_2)}$.

Remark 4: The above result suggests that tuning power allocation to satisfy $\rho < \rho_{\max}$ results in better performance for both users. However, tuning $\rho \geq \rho_{\max}$ causes significant loss in the performance during downlink transmission. Therefore, similar to the fixed decoding order approach, the dynamic decoding order scheme offers remarkable outage performance in the downlink when focusing on improving that of the weaker receiver.

$$P(\phi_n, \phi_t; y, z) = Q(y\phi_n, \phi_t; z) - \frac{1}{\Gamma(M_n m_n)\Gamma(M_t m_t)} \left(\frac{m_t}{\mu_t}\right)^{M_t m_t} \left(\frac{m_n y}{\mu_n}\right)^{M_n m_n} \left(\frac{m_t}{\mu_t} + \frac{m_n y}{\mu_n}\right)^{-M_t m_t - M_n m_n} \times \sum_{i=1}^{\infty} \sum_{j=0}^{i-1} \eta(M_n m_n; i, j) \left(\frac{m_n y}{\mu_n}\right)^{j} \left(\frac{m_t}{\mu_t} + \frac{m_n y}{\mu_n}\right)^{i-j} \Gamma\left(M_t m_t + M_n m_n - (i-j); \left[\frac{m_t}{\mu_t} + \frac{m_n y}{\mu_n}\right] z\right) \tag{25}$$

C. ASYMPTOTIC AND DIVERSITY ANALYSIS

In this subsection, we study asymptotic behaviors as well as the diversity order of each destination under the assumption of equal transmit power. The asymptotic results can then be viewed as approximations for the outage probability at each destination in the high transmit power regime. The diversity orders, under various settings, are derived to gain deeper insights into the proposed system.

1) ASYMPTOTIC ANALYSIS

Many results obtained in this subsection are obtained with the help of the following asymptotic identities [48], [50]

$$\gamma(a;x) \to \frac{\Gamma(a)}{\Gamma(a+1)}x^a, \quad x \to 0, \tag{32a}$$

$$\Gamma(a;x) \to \Gamma(a), \quad x \to 0. \tag{32b}$$

Under the assumption that $\bar{P}_1 = \bar{P}_2 = \bar{P}_R \triangleq \bar{P}$, the following corollaries are then provided to simplify the results in the previous section as well as support the upcoming analysis.

Corollary 2: When $\bar{P} \to \infty$, the asymptotic expression for the defined function $Q(\phi_n, \phi_t; z)$ is given by

$$Q_\infty(\phi_n, \phi_t; z) = Q(\phi_n, \phi_t; 0) - \frac{(\frac{m_t z}{\mu_t})^{M_t m_t}}{\Gamma(M_t m_t + 1)}. \tag{33}$$

Corollary 3: When $\bar{P} \to \infty$, the asymptotic expression for the defined function $P(\phi_n, \phi_t; y, z)$ is given by

$$P_\infty(\phi_n, \phi_t; y, z) = Q_\infty(y\phi_n, \phi_t; z) - A_{n,t}(y)\left(\frac{m_n y}{\mu_n} + \frac{m_t}{\mu_t}\right), \tag{34}$$

where $A_{n,t}(y)$ is defined as follows for ease of analysis

$$A_{n,t}(y) \triangleq \frac{\Gamma(M_n m_n + M_t m_t - 1)}{\Gamma(M_n m_n)\Gamma(M_t m_t)} \times \frac{(m_n \mu_t y)^{M_n m_n}(m_t \mu_n)^{M_t m_t}}{(m_n \mu_t y + m_t \mu_n)^{M_n m_n + M_t m_t}}.$$

Using (33) and (34), the outage probability at the relay can be asymptotically expressed by (35a)-(35c), as shown at the bottom of the page. It is worth pointing out that (33) is derived by neglecting $\Delta(\cdot)$ in (18) and then apply (32a) to approximate $F_{\phi_t}(z)$, whereas (33) is obtained by only considering $i = 1$ in (25). In addition, the probabilities Pr_1 and Pr_2 in (27) can be approximated in the following corollary.

Corollary 4: When $\bar{P} \to \infty$, thus $\lambda_n \to \infty$, the probabilities Pr_1 and Pr_2 in (28) can be asymptotically expressed by

$$\mathrm{Pr}_1 \to Q(\psi_t, \psi_n; 0) - \frac{(\frac{k_n \vartheta_n}{\lambda_n})^{K_n k_n}}{\Gamma(K_n K_n + 1)} \text{ and} \tag{36}$$

$$\mathrm{Pr}_2 \to Q(\psi_n, \psi_t; 0), \tag{37}$$

respectively. Note that $Q(\phi_n, \phi_t; 0) + Q(\phi_t, \phi_n; 0) = 1$.

2) DIVERSITY ORDER

The diversity order can be computed by [48]

$$\mathcal{O}_{D_n} = -\lim_{\bar{P}\to\infty} \frac{\log_{10}(P_{D_n}^{out}(\bar{P}))}{\log_{10}(\bar{P})}, \tag{38}$$

in which $P_{D_n}^{out}(\bar{P}) \triangleq 1-(1-P_R^{out}(\bar{P}))(1-P_{R\to D_n}^{out}(\bar{P}))$ is merely $P_{D_n}^{out}$ in (13) expressed as a function of the transmit power $\bar{P}$. In an another perspective, if the term $P_{D_n}^{out}(\bar{P})$ is presented as $a\bar{P}^{-b}$, in which a and b are $\bar{P}$-independent non-negative constants, then $\mathcal{O}_{D_n} = b$ which implies that increasing $\bar{P}$ by p (dB) in the high transmit SNR regime will decrease the outage by $b \times p$ (dB). In addition, the diversity order can be approximately calculated as

$$\mathcal{O}_{D_n} \approx \log_p(P_{D_n}^{out}(\bar{P})) - \log_p(P_{D_n}^{out}(p\bar{P})), \quad p > 0, \tag{39}$$

in which $\bar{P}$ should have relatively high value to obtain a more precise result.

Due to the many cases of $P_R^{out}(\bar{P})$ in (25) and $P_{R\to D_n}^{out}(\bar{P})$ in (30), there are a total of 36 cases for the $\mathcal{O}_{D_n}$, in which we examined that most cases result zero diversity order at both D_1 and D_2. By assuming that $\rho < \rho_{\max}$, which is the most effective power allocation for the downlink, thus $P_{R\to D_n}^{out}(\bar{P}) \to 1 - (\mathrm{Pr}_1^\infty + \mathrm{Pr}_2^\infty)$ and can be expressed as

$$P_{R\to D_n}^{out}(\bar{P}) \propto \bar{P}^{-K_n k_n}. \tag{40}$$

$$P_R^{out}(\bar{P}) \to \frac{(\frac{m_1\tau_1}{\mu_1})^{M_1 m_1}}{\Gamma(M_1 m_1 + 1)} + \frac{(\frac{m_2\tau_2}{\mu_2})^{M_2 m_2}}{\Gamma(M_2 m_2 + 1)}, \quad \tau_1 < 1,\ \tau_2 < 1, \tag{35a}$$

$$P_R^{out}(\bar{P}) \to Q(\phi_n, \phi_t; 0) - Q(\tau_n\phi_n, \phi_t; 0) + \frac{(\frac{m_1\tau_1}{\mu_1})^{M_1 m_1}}{\Gamma(M_1 m_1 + 1)} + \frac{(\frac{m_2\tau_2}{\mu_2})^{M_2 m_2}}{\Gamma(M_2 m_2 + 1)} + A_{n,t}(\tau_n)\left(\frac{m_n\tau_n}{\mu_n} + \frac{m_t}{\mu_t}\right), \quad \tau_n \geq 1,\ \tau_t < 1, \tag{35b}$$

$$P_R^{out}(\bar{P}) \to 1 - Q(\tau_1\phi_1, \phi_2; 0) - Q(\tau_2\phi_2, \phi_1; 0) + \frac{(\frac{m_1\tau_1}{\mu_1})^{M_1 m_1}}{\Gamma(M_1 m_1 + 1)} + \frac{(\frac{m_2\tau_2}{\mu_2})^{M_2 m_2}}{\Gamma(M_2 m_2 + 1)} + A_{1,2}(\tau_1)\left(\frac{m_1\tau_1}{\mu_1} + \frac{m_2}{\mu_2}\right) + A_{2,1}(\tau_2)\left(\frac{m_2\tau_2}{\mu_2} + \frac{m_1}{\mu_1}\right), \quad \tau_1 \geq 1,\ \tau_2 \geq 1 \tag{35c}$$

In addition, from (35a)-(35c), the probability $P_R^{out}(\bar{P})$ can also be expressed as

$$P_R^{out}(\bar{P}) \propto \begin{cases} \bar{P}^{-\beta}, & \tau_1 < 1, \tau_2 < 1 \\ \bar{P}^{-\min(\beta,1)}, & \tau_1 = 1, \tau_2 < 1 \\ \bar{P}^{-\min(\beta,1)}, & \tau_1 < 1, \tau_2 = 1 \\ \bar{P}^{0}, & \text{otherwise} \end{cases} \quad (41)$$

in which $\beta \triangleq \min(M_1\, m_1, M_2\, m_2)$.

Upon substituting (A.2) and (A.1) into (38), the results of the $\mathcal{O}_{D_n}$ can be summarized in table 1.

TABLE 1. Diversity order at D_n with $\rho < \rho_{\max}$.

	$\bar{R}_1 < 0.5$ (bps/Hz)	$\bar{R}_1 = 0.5$ (bps/Hz)
$\bar{R}_2 < 0.5$ (bps/Hz)	$\min(\beta, K_n k_n)$	$\min(\beta, K_n k_n, 1)$
$\bar{R}_2 = 0.5$ (bps/Hz)	$\min(\beta, K_n k_n, 1)$	$\min(\beta, K_n k_n, 1)$
$\mathcal{O}_{D_n} = 0$ if $\bar{R}_1 > 0.5$ or $\bar{R}_2 > 0.5$		

Remark 5: It can be viewed from the above table that for $R_1 > 0.5$ (bps/Hz) or $R_2 > 0.5$ (bps/Hz), not only both D_n experience more serious performance loss due to higher demand, but the performance is also limited by a floor level due to zero diversity order. However, as the services of the paired D_n are less demanding till $R_1, R_2 \leq 0.5$ (bps/Hz), the performance gain of the system can be regulated effectively by improving the transmit power at the transmitters, i.e., the sources and the relay.

IV. NUMERICAL RESULTS

In this section, we demonstrate the outage performance of the proposed uplink/downlink NOMA over Nakagami-m fading channels. In the simulations, the outage probability depends on dynamic decoding order scheme. As a default, the path loss exponent is $\alpha = 2$, the power allocation factor is $\rho = 0.3$ and all S_n, D_n are assumed to have the same number of antennas, i.e., $M_1 = M_2 = K_1 = K_2 \triangleq N$. It should be noted that increasing $\alpha > 2$ gradually deteriorates the system performance but does not affect the diversity order at both destinations.

Moreover, the analytical curves represent the outage probability $P_{D_n}^{out}$ in (13), in which P_R^{out} is in (26) and $P_{R\to D_n}^{out}$ is in (31). On the other hand, the simulation curves also use $P_{D_n}^{out}$ in (13), but P_R^{out} and $P_{R\to D_n}^{out}$ are obtained from (11) and (12), respectively. Further, the asymptotic curves use $P_R^{out}(\bar{P})$ in (35a)-(35c) and $P_{R\to D_n}^{out}(\bar{P})$ in (31) with $\Pr_1$ in (37) and $\Pr_2$ in (38).

The given results in Fig. 2−Fig. 4 adopt the settings $(m_1; d_1) = (0.8; 6)$, $(m_2; d_2) = (1.6; 2)$, $(k_1; l_1) = (1.6; 2)$, $(k_2; l_2) = (0.8; 6)$. Fig. 2 demonstrates the outage probability in terms of the average SNR ($\bar{P}$). It can be observed clearly that the exact outage probability and the Monte Carlo simulation curves are matched precisely. The derived outage probability expressions are valid since the dotted curves indicates the asymptotic outage probability. The asymptotic

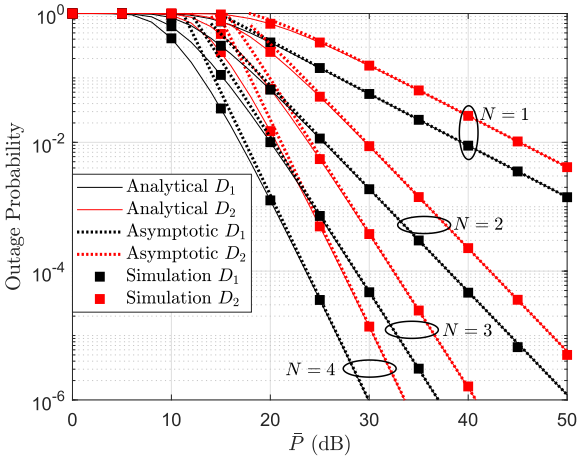

FIGURE 2. Outage probability at D_1 and D_2 versus the average transmit SNR $\bar{P}$ (dB), in which $\bar{R}_1 = \bar{R}_2 = 0.45$ (bps/Hz).

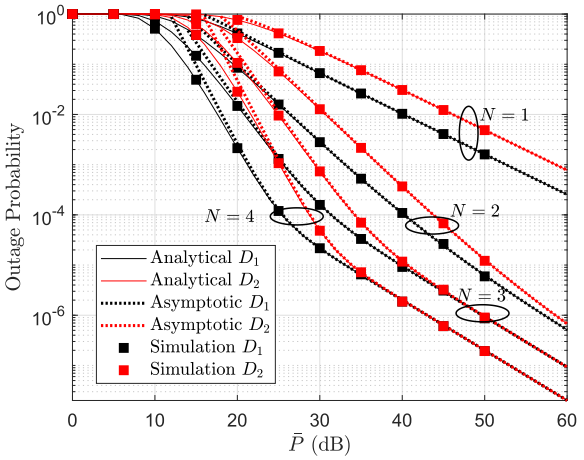

FIGURE 3. Outage probability at D_1 and D_2 versus the average transmit SNR $\bar{P}$ (dB), in which $\bar{R}_1 = \bar{R}_2 = 0.5$ (bps/Hz).

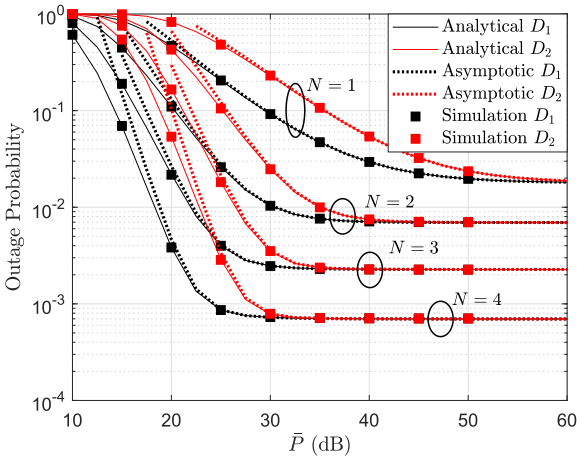

FIGURE 4. Outage probability at D_1 and D_2 versus the average transmit SNR $\bar{P}$ (dB), in which $\bar{R}_1 = \bar{R}_2 = 0.55$ (bps/Hz).

curves well approximate the exact performance curves in some ranges of SNR, especially when $\bar{P}$ is beyond 30 (dB). It is observed that increasing $\bar{P}$ by 10 (dB) results in the decrease

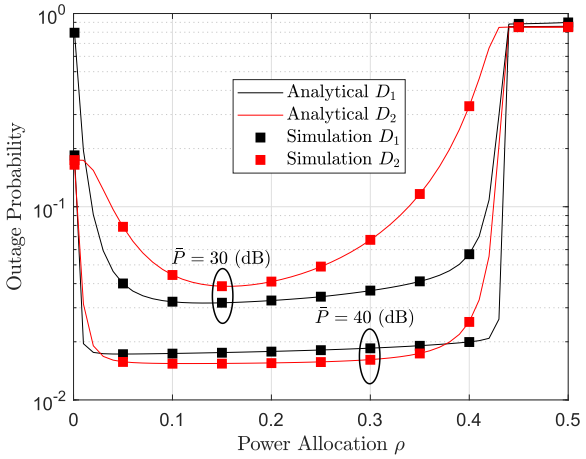

FIGURE 5. Outage probability at D_1 and D_2 versus the minimum power allocation ρ, in which $\bar{R}_1 = 0.4$ (bps/Hz), $\bar{R}_2 = 0.6$ (bps/Hz) and $N = M = 1$.

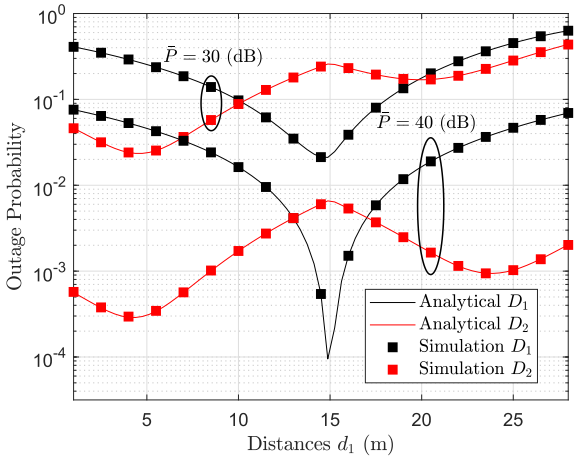

FIGURE 6. Outage probability at D_1 and D_2 versus the distance d_1, in which $l_1 = |15 - d_1|$, $d_2 = l_1$ and $l_2 = d_1$.

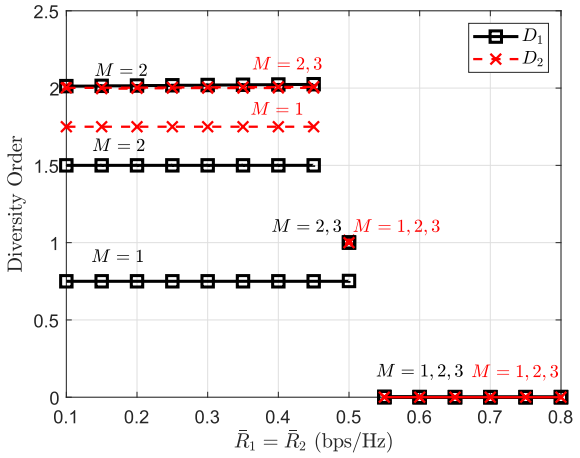

FIGURE 7. An illustration of the diversity order at each destination.

of the $P_{D_n}^{out}$ by 8 (dB), 16 (dB), 24 (dB) and 32 (dB) when $N = 1, N = 2, N = 3$ and $N = 4$, respectively. The reason is that all target data rates are below 0.5 (bps/Hz), thus the diversity order at the n-th destination (D_n) are determined by the weakest link and the number of antennas as shown in Table 1.

Fig. 3 shows the similar trends with Fig. 2 for outage performance of both destinations, however, the target rates are $\bar{R}_1 = \bar{R}_2 = 0.5$ (bps/Hz). Surprisingly, the diversity order at both destinations are dropped significantly where the outage probabilities are only decreased by 10 (dB) for $N = 2, 3, 4$ comparing to Fig. 2. Similar to Fig. 2, the simulation curves well matched the analytical curves which again validates our analysis.

Fig. 4 indicates that, the outage probabilities go saturation lines at high SNR region. The main reason is that the diversity order is zero, and then it can not improve outage performance at high SNR as two previous simulation results (reported in Fig. 2 and Fig. 3). In this case, the main approach to improve the performance is to deploy more antennas with the cost of higher signalling overhead. In addition, the destinations exhibit same outage performance when the average SNR exceeds 40 (dB).

In Fig. 5−Fig. 7, we assume that $M_1 = M_2 = N$, $K_1 = K_2 = M$, $(m_1; d_1) = (3; 6)$, $(m_2; d_2) = (2; 2)$, $(k_1; l_1) = (0.75; 2)$ and $(k_2; l_2) = (1.75; 6)$. Fig. 5 demonstrates how power allocation factors make influence on outage performance of both destinations. This figure shows the outage performance versus the power allocation for the stronger receiver, i.e., the destination having higher channel power gain. It can be seen that at the value $\rho \geq \rho_{\max} \approx 0.43$, the performance at both downlink receivers significantly deteriorates as explained in Remark 4.

As can be seen in Fig. 6, we consider another channel condition, i.e., the source-relay link is statistically worse than the relay-user link. The Euclidean distance d_1 is set to be in range from 1 (m) to 28 (m). In this case, the optimal outage probability in the UL/DL NOMA system can be achieved. When the source S_1 is located close to the relay, the outage performance of D_1 can be improved significantly compared with that for D_2. The results show that the locations of these nodes make crucial impacts on outage performance of two destinations.

In Fig. 7, the diversity order at both destinations are clearly presented under different M. The results are obtained by using (39) at $\bar{P} \geq 55$ (dB) and $p = 5$ (dB). In the range of $\bar{R}_n \in [0.1, 0.5)$ (bps/Hz), the diversity orders at D_1 is doubled when M increases from $M = 1$ to $M = 2$ but then only raise by 0.5 when further increases M by one. In addition, the diversity order at D_2 only raises by 0.5 when increases M from $M = 2$ to $M = 3$ whereas no improvement is observed when further increases M. At the point $\bar{R}_n = 0.5$ (bps/Hz), both orders are bounded by one and cannot exceed this value even with increasing M. In the worst scenario, where $\bar{R}_n \in (0.5, 0.8]$ (bps/Hz), zero diversity orders are observed at both destinations. The results thus are complied with Table 1 which validates the analysis for diversity order.

V. CONCLUSION

In this paper, we have investigated a new UL/DL NOMA system where two users communicate with two destinations via a common relay. The destination users intend to receive information in DL which corresponds to the transmitted signals in UL and such model is more effectively with architecture of SIMO and MISO. By analyzing the outage probabilities with high transmit SNR, we have further pointed out that the outage behavior in both cases of received signals mainly depend on the target rates and location of nodes in NOMA networks. The parameters of fading channels are also evaluated in many scenarios. The main results demonstrated that the optimal of outage probability for UL/DL NOMA can be achieved by adjust power allocation factors. This proposed dynamic decoding order benefits to NOMA system to satisfy fairness and improve outage performance.

APPENDIX A
PROOF OF PROPOSITION 1

The probability $Q(\phi_n, \phi_t; z)$ can be rewritten as

$$Q(\phi_n, \phi_t; z) = \Pr\{\phi_n > \phi_t\} - \Pr\{\phi_t < z\} + \Pr\{\phi_n > \phi_t, \phi_t < z\}. \quad \text{(A.1)}$$

In the first probability, the term $\frac{\phi_t}{\phi_n}$ is the ratio of two independent Gamma RVs, in which

$$\phi_n \sim \mathcal{G}(M_n m_n, \mu_n/m_n) \text{ and}$$
$$\phi_t \sim \mathcal{G}(M_t m_t, \mu_t/m_t).$$

Hence, the term $\frac{\phi_n}{\phi_t}$ can be statistically characterized by the Beta prime distribution [52]. Specifically, the CDF of the term $\frac{\phi_t}{\phi_n}$ can be given by

$$F(\phi) = \frac{(\frac{\phi}{\lambda})^{\alpha} {}_2F_1\left(\alpha, \alpha+\beta; \alpha+1; -\frac{\phi}{\lambda}\right)}{\alpha \mathbf{B}(\alpha; \beta)}, \quad \text{(A.2)}$$

in which $\lambda \triangleq m_n\mu_t/m_t\mu_n$, $\alpha \triangleq M_t m_t$ and $\beta \triangleq M_n m_n$.

Besides, the probability $\Pr\{\phi_n > \phi_t\}$ can be viewed as $Q(\phi_n, \phi_t; 0)$ due to (14) or, equivalently, the CDF $F(\phi)$ in the above equation measured at $\phi = 1$. The second probability in (A.1) is simply $F_{\phi_t}(z)$ presented by (17).

The third probability in (A.1), denoted by $\Pr_3$, can be derived as

$$\Pr_3 = \int_0^z f_{\phi_t}(y) F_{\phi_n}(y) dy. \quad \text{(A.3)}$$

By applying Gaussian-Chebyshev quadrature [49] we then obtain (20). With the aforementioned results, we then obtain (19) as well as (18) which concludes the proof.

APPENDIX B
PROOF OF PROPOSITION 2

The general formula for the Taylor series of the function $\Gamma(v; z)$ at the expansion point $z_0 \neq 0$ is defined as

$$\Gamma(v; z) = \sum_{i=0}^{\infty} \frac{1}{i!} \left[\frac{\partial^i}{\partial z^i}\Gamma(v; z)\right]\Big|_{z \to z_0} (z - z_0)^i. \quad \text{(B.1)}$$

In addition, for $i \geq 1$, the i-th derivative of $\Gamma(v; z)$ can be expressed as

$$\frac{\partial^i}{\partial z^i}\Gamma(v; z) \overset{(a)}{=} -(i-1)! z^{v-i} e^{-z} L_{i-1}^{v-i}(z) \quad \text{(B.2)}$$

$$\overset{(b)}{=} -(i-1)! z^{v} e^{-z} \sum_{j=0}^{i-1} \frac{(v-i+j+1)_{i-j-1}}{j!(i-j-1)!} \frac{1}{z^{i-j}}, \quad \text{(B.3)}$$

in which (a) is due to [51, Eq. (1.8.1.17)] and (b) is due to the definition of the Laguerre polynomial $L_n^a(z)$ as [47, Eq. (8.970.1)]

$$L_n^a(z) = \sum_{i=0}^{n} \binom{n-a}{n-i} \frac{(-1)^i}{i!} x^i, \quad \text{(B.4)}$$

$$= \sum_{i=0}^{n} \frac{(a+i+1)_{n-i}}{(n-i)!} \frac{(-1)^i}{i!} x^i, \quad \text{(B.5)}$$

in which the last equality is introduced for $n - a$ taking real values. Finally, substituting (B.3) into (B.1), we then obtain the desired result in (24).

APPENDIX C
PROOF OF PROPOSITION 3

Denoting the first and second probability in (11) by Θ_1 and Θ_2, respectively, thus

$$\Theta_1 = \Pr\{\phi_1 > \max(\tau_1(\phi_2+1), \phi_2), \phi_2 > \tau_2\}, \quad \text{(C.1)}$$

where the analysis for this probability can be divided into the two main cases 1) $\tau_1 \geq 1$ and 2) $\tau_1 < 1$.

In the first case, $\max(\tau_1(\phi_2+1), \phi_2) = \tau_1(\phi_2+1)$, the probability Θ_1 becomes

$$\Theta_1 = \Pr\{\phi_1 > \tau_1(\phi_2+1), \phi_2 > \tau_2\} = P(\phi_1, \phi_2; \tau_1, \tau_2). \quad \text{(C.2)}$$

In the second case, the analysis of Θ_1 can be further divided into two subcases.

+ *Subcase 1*: $\tau_1(\phi_2+1) > \phi_2$ or, equivalently, $\tau_2 < \phi_2 < \frac{\tau_1}{1-\tau_1}$, thus

$$\Theta_1 = \Pr\{\phi_1 > \tau_1(\phi_2+1), \phi_2 > \tau_2\} - \Pr\left\{\phi_1 > \tau_1(\phi_2+1), \phi_2 > \frac{\tau_1}{1-\tau_1}\right\} = P(\phi_1, \phi_2; \tau_1, \tau_2) - P\left(\phi_1, \phi_2; \tau_1, \frac{\tau_1}{1-\tau_1}\right) \quad \text{(C.3)}$$

with $\tau_2 < \frac{\tau_1}{1-\tau_1}$ and $\tau_1 < 1$.

+ *Subcase 2*: $\tau_1(\phi_2+1) < \phi_2$ or $\phi_2 \geq \max(\tau_2, \frac{\tau_1}{1-\tau_1})$, thus

$$\Theta_1 = \Pr\{\phi_1 > \phi_2, \phi_2 > \theta_2\} = Q(\phi_1, \phi_2; \theta_2). \quad \text{(C.4)}$$

Combining (C.2), (C.3) and (C.4) with a note that $\frac{\tau_1}{1-\tau_1} = \theta_2$ when $\tau_2 < \frac{\tau_1}{1-\tau_1}$, we then obtain

$$\Theta_1 = P(\phi_1, \phi_2; \tau_1, \tau_2) + \begin{cases} Q(\phi_1, \phi_2; \theta_2) - P(\phi_1, \phi_2; \tau_1, \theta_2), & \tau_1 < 1 \\ 0, & \tau_1 \geq 1 \end{cases} \quad \text{(C.5)}$$

The probability Θ_2 can be derived in a similar manner as Θ_1 and thus is neglected. Finally, by combining Θ_1 and Θ_2 we then obtain the desired result.

REFERENCES

[1] L. Dai, B. Wang, Y. Yuan, S. Han, C.-L. I, and Z. Wang, "Non-orthogonal multiple access for 5G: Solutions, challenges, opportunities, and future research trends," *IEEE Commun. Mag.*, vol. 53, no. 9, pp. 74–81, Sep. 2015.

[2] T.-L. Nguyen and D.-T. Do, "Exploiting impacts of intercell interference on SWIPT-assisted non-orthogonal multiple access," *Wireless Commun. Mobile Comput.*, vol. 2018, Nov. 2018, Art. no. 2525492.

[3] V. W. S. Wong, R. Schober, D. W. K. Ng, and L.-C. Wang, *Key Technologies for 5G Wireless Systems*. Cambridge, U.K.: Cambridge Univ. Press, 2017.

[4] Z. Wei, L. Yang, D. W. K. Ng, J. Yuan, and L. Hanzo, "On the performance gain of NOMA over OMA in uplink communication systems," *IEEE Trans. Commun.*, vol. 68, no. 1, pp. 536–568, Jan. 2020.

[5] D.-T. Do, C.-B. Le, and B. M. Lee, "Robust transmit antenna design for performance improvement of cell-edge users: Approach of NOMA and outage/ergodic capacity analysis," *Sensors*, vol. 19, no. 22, p. 4907, Nov. 2019.

[6] T.-L. Nguyen and D.-T. Do, "Power allocation schemes for wireless powered NOMA systems with imperfect CSI: An application in multiple antenna-based relay," *Int. J. Commun. Syst.*, vol. 31, no. 15, p. e3789, Oct. 2018.

[7] S. M. R. Islam, M. Zeng, O. A. Dobre, and K.-S. Kwak, "Resource allocation for downlink NOMA systems: Key techniques and open issues," *IEEE Wireless Commun.*, vol. 25, no. 2, pp. 40–47, Apr. 2018.

[8] F. Fang, Z. Ding, W. Liang, and H. Zhang, "Optimal energy efficient power allocation with user fairness for uplink MC-NOMA systems," *IEEE Wireless Commun. Lett.*, vol. 8, no. 4, pp. 1133–1136, Aug. 2019.

[9] M. S. Ali, E. Hossain, and D. I. Kim, "Non-orthogonal multiple access (NOMA) for downlink multiuser MIMO systems: User clustering, beamforming, and power allocation," *IEEE Access*, vol. 5, pp. 565–577, Mar. 2017.

[10] D.-T. Do and M.-S. Van Nguyen, "Device-to-device transmission modes in NOMA network with and without wireless power transfer," *Comput. Commun.*, vol. 139, pp. 67–77, May 2019.

[11] S. M. R. Islam, N. Avazov, O. A. Dobre, and K.-S. Kwak, "Power-domain non-orthogonal multiple access (NOMA) in 5G systems: Potentials and challenges," *IEEE Commun. Surveys Tuts.*, vol. 19, no. 2, pp. 721–742, 2nd Quart., 2017.

[12] D.-T. Do, M. Vaezi, and T.-L. Nguyen, "Wireless powered cooperative relaying using NOMA with imperfect CSI," in *Proc. IEEE Globecom Workshops (GC Wkshps)*, Abu Dhabi, United Arab Emirates, Dec. 2018, pp. 1–6.

[13] D.-T. Do and A.-T. Le, "NOMA based cognitive relaying: Transceiver hardware impairments, relay selection policies and outage performance comparison," *Comput. Commun.*, vol. 146, pp. 144–154, Oct. 2019.

[14] D.-T. Do, A.-T. Le, and A. B. M. Lee, "On performance analysis of underlay cognitive radio-aware hybrid OMA/NOMA networks with imperfect CSI," *Electronics*, vol. 8, no. 7, p. 819, Jul. 2019.

[15] A. Shahini and N. Ansari, "NOMA aided narrowband IoT for machine type communications with user clustering," *IEEE Internet Things J.*, vol. 6, no. 4, pp. 7183–7191, Aug. 2019.

[16] A. E. Mostafa, Y. Zhou, and V. W. S. Wong, "Connection density maximization of narrowband IoT systems with NOMA," *IEEE Trans. Wireless Commun.*, vol. 18, no. 10, pp. 4708–4722, Oct. 2019.

[17] W. Mei and R. Zhang, "Uplink cooperative NOMA for cellular-connected UAV," *IEEE J. Sel. Topics Signal Process.*, vol. 13, no. 3, pp. 644–656, Jun. 2019.

[18] X. Li, Q. Wang, H. Peng, H. Zhang, D.-T. Do, K. M. Rabie, R. Kharel, and C. C. Cavalcante, "A unified framework for HS-UAV NOMA networks: Performance analysis and location optimization," *IEEE Access*, vol. 8, pp. 13329–13340, 2020.

[19] J. Zhu, J. Wang, Y. Huang, S. He, X. You, and L. Yang, "On optimal power allocation for downlink non-orthogonal multiple access systems," *IEEE J. Sel. Areas Commun.*, vol. 35, no. 12, pp. 2744–2757, Dec. 2017.

[20] J. He and Z. Tang, "Low-complexity user pairing and power allocation algorithm for 5G cellular network non-orthogonal multiple access," *Electron. Lett.*, vol. 53, no. 9, pp. 626–627, Apr. 2017.

[21] M. Pischella and D. Le Ruyet, "NOMA-relevant clustering and resource allocation for proportional fair uplink communications," *IEEE Wireless Commun. Lett.*, vol. 8, no. 3, pp. 873–876, Jun. 2019.

[22] Y. Sun, D. W. K. Ng, Z. Ding, and R. Schober, "Optimal joint power and subcarrier allocation for full-duplex multicarrier non-orthogonal multiple access systems," *IEEE Trans. Commun.*, vol. 65, no. 3, pp. 1077–1091, Mar. 2017.

[23] J. Zhao, Y. Liu, K. K. Chai, A. Nallanathan, Y. Chen, and Z. Han, "Spectrum allocation and power control for non-orthogonal multiple access in HetNets," *IEEE Trans. Wireless Commun.*, vol. 16, no. 9, pp. 5825–5837, Sep. 2017.

[24] M. Bashar, K. Cumanan, A. G. Burr, H. Q. Ngo, L. Hanzo, and P. Xiao, "On the performance of cell-free massive MIMO relying on adaptive NOMA/OMA mode-switching," *IEEE Trans. Commun.*, vol. 68, no. 2, pp. 792–810, Feb. 2020.

[25] A. S. Marcano and H. L. Christiansen, "Impact of NOMA on network capacity dimensioning for 5G HetNets," *IEEE Access*, vol. 6, pp. 13587–13603, 2018.

[26] O. Abbasi, A. Ebrahimi, and N. Mokari, "NOMA inspired cooperative relaying system using an AF relay," *IEEE Wireless Commun. Lett.*, vol. 8, no. 1, pp. 261–264, Feb. 2019.

[27] M. F. Kader and S. Y. Shin, "Coordinated direct and relay transmission using uplink NOMA," *IEEE Wireless Commun. Lett.*, vol. 7, no. 3, pp. 400–403, Jun. 2018.

[28] M. F. Kader, M. B. Shahab, and S. Y. Shin, "Exploiting non-orthogonal multiple access in cooperative relay sharing," *IEEE Commun. Lett.*, vol. 21, no. 5, pp. 1159–1162, May 2017.

[29] M. F. Kader, S. Y. Shin, and V. C. M. Leung, "Full-duplex non-orthogonal multiple access in cooperative relay sharing for 5G systems," *IEEE Trans. Veh. Technol.*, vol. 67, no. 7, pp. 5831–5840, Jul. 2018.

[30] S. M. Ibraheem, W. Bedawy, W. Saad, and M. Shokair, "Outage performance of NOMA-based DF relay sharing networks over Nakagami-*m* fading channels," in *Proc. 13th Int. Conf. Comput. Eng. Syst. (ICCES)*, Cairo, Egypt, Dec. 2018, pp. 512–517.

[31] R. Zhang and L. Hanzo, "A unified treatment of superposition coding aided communications: Theory and practice," *IEEE Commun. Surveys Tuts.*, vol. 13, no. 3, pp. 503–520, 3rd Quart., 2011.

[32] J. Zhang, L. Zhu, Z. Xiao, X. Cao, D. O. Wu, and X.-G. Xia, "Optimal and sub-optimal uplink NOMA: Joint user grouping, decoding order, and power control," *IEEE Wireless Commun. Lett.*, vol. 9, no. 2, pp. 254–257, Feb. 2020.

[33] Y. Gao, B. Xia, K. Xiao, Z. Chen, X. Li, and S. Zhang, "Theoretical analysis of the dynamic decode ordering SIC receiver for uplink NOMA systems," *IEEE Commun. Lett.*, vol. 21, no. 10, pp. 2246–2249, Oct. 2017.

[34] Y. Gao, B. Xia, Y. Liu, Y. Yao, K. Xiao, and G. Lu, "Analysis of the dynamic ordered decoding for uplink NOMA systems with imperfect CSI," *IEEE Trans. Veh. Technol.*, vol. 67, no. 7, pp. 6647–6651, Jul. 2018.

[35] Y. Liu, M. Derakhshani, and S. Lambotharan, "Outage analysis and power allocation in uplink non-orthogonal multiple access systems," *IEEE Commun. Lett.*, vol. 22, no. 2, pp. 336–339, Feb. 2018.

[36] J. Wang, B. Xia, K. Xiao, Y. Gao, and S. Ma, "Outage performance analysis for wireless non-orthogonal multiple access systems," *IEEE Access*, vol. 6, pp. 3611–3618, 2018.

[37] B. Xia, J. Wang, K. Xiao, Y. Gao, Y. Yao, and S. Ma, "Outage performance analysis for the advanced SIC receiver in wireless NOMA systems," *IEEE Trans. Veh. Technol.*, vol. 67, no. 7, pp. 6711–6715, Jul. 2018.

[38] A. Annamalai and C. Tellambura, "Error rates for Nakagami-*m* fading multichannel reception of binary and M-ary signals," *IEEE Trans. Commun.*, vol. 49, no. 1, pp. 58–68, Jan. 2001.

[39] S. Kumar, "Approximate outage probability and capacity for κ-μ shadowed fading," *IEEE Wireless Commun. Lett.*, vol. 4, no. 3, pp. 301–304, Jun. 2015.

[40] J. F. Paris, "Statistical characterization of $\kappa-\mu$ shadowed fading," *IEEE Trans. Veh. Technol.*, vol. 63, no. 2, pp. 518–526, Feb. 2014.

[41] J. Zhang, E. Björnson, M. Matthaiou, D. W. K. Ng, H. Yang, and D. J. Love, "Prospective multiple antenna technologies for beyond 5G," *IEEE J. Sel. Areas Commun.*, early access, Jun. 10, 2020, doi: 10.1109/JSAC.2020.3000826.

[42] A. Afana, V. Asghari, A. Ghrayeb, and S. Affes, "On the performance of cooperative relaying spectrum-sharing systems with collaborative distributed beamforming," *IEEE Trans. Commun.*, vol. 62, no. 3, pp. 857–871, Mar. 2014.

[43] S. C. Liew, L. Lu, and S. Zhang, "A primer on physical-layer network coding," *Synth. Lectures Commun. Netw.*, vol. 8, no. 1, pp. 1–218, 2015.

[44] A. Afana, V. Asghari, A. Ghrayeb, and S. Affes, "On the performance of cooperative relaying spectrum-sharing systems with collaborative distributed beamforming," *IEEE Trans. Commun.*, vol. 62, no. 3, pp. 857–871, Mar. 2014.
[45] J. Yang, X. Wu, H. M. Nguyen, and J. Ding, "Outage probability of scheduled MRT scheme in cognitive MISO networks with imperfect CSI," *IET Commun.*, vol. 12, no. 15, pp. 1919–1924, Sep. 2018.
[46] G. Zhu, C. Zhong, H. A. Suraweera, Z. Zhang, and C. Yuen, "Outage probability of dual-hop multiple antenna AF systems with linear processing in the presence of co-channel interference," *IEEE Trans. Wireless Commun.*, vol. 13, no. 4, pp. 2308–2321, Apr. 2014.
[47] A. Jeffrey and D. Zwillinger, *Table of Integrals, Series, and Products*. New York, NY, USA: Academic, 2007.
[48] X. Yue, Y. Liu, S. Kang, and A. Nallanathan, "Performance analysis of NOMA with fixed gain relaying over Nakagami-*m* fading channels," *IEEE Access*, vol. 5, pp. 5445–5454, 2017.
[49] E. Hildebrand, *Introduction to Numerical Analysis*. New York, NY, USA: Dover, 1987.
[50] J. Men, J. Ge, and C. Zhang, "Performance analysis of non-orthogonal multiple access for relaying networks over Nakagami-*m* fading channels," *IEEE Trans. Veh. Technol.*, vol. 66, no. 2, pp. 1200–1208, Feb. 2016.
[51] Y. A. Brychkov, *Handbook of Special Functions: Derivatives, Integrals, Series and Other Formulas*. London, U.K.: Chapman & Hall, 2008.
[52] A. Bekker, J. Roux, and T. Pham-Gia, "The type I distribution of the ratio of independent 'Weibullized' generalized beta-prime variables," *Stat. Papers*, vol. 50, no. 2, pp. 323–338, Mar. 2009.

DINH-THUAN DO (Senior Member, IEEE) received the B.S., M.Eng., and Ph.D. degrees in communications engineering from Vietnam National University (VNUHCM), in 2003, 2007, and 2013, respectively.

He was a Visiting Ph.D. Student with the Communications Engineering Institute, National Tsing Hua University, Taiwan, from 2009 to 2010. Prior to joining Ton Duc Thang University, he was a Senior Engineer at VinaPhone Mobile Network, from 2003 to 2009. He was a recipient of the Golden Globe Award from the Vietnam Ministry of Science and Technology, in 2015 (Top 10 excellent young scientists nationwide). His research interests include signal processing in wireless communications networks, cooperative communications, non-orthogonal multiple access, full-duplex transmission, and energy harvesting. He published over 70 SCI/SCIE journal articles, four book chapters, and one sole author book. He is currently serving as an associate editor for 6 journals, in which mainly SCIE journals are *EURASIP Journal on Wireless Communications and Networking*, *Computer Communications* (Elservier), *Electronics*, and *KSII Transactions on Internet and Information Systems*.

THANH-LUAN NGUYEN received the B.S. degree (Hons.) from the Ho Chi Minh City University of Technology and Education, Vietnam, in 2016. He is currently a Research Assistant with the Faculty of Electronics Technology, Industrial University of Ho Chi Minh City (IUH). His research interests include NOMA, energy harvesting, generalized channels, and other emerging technologies.

SABIT EKIN (Member, IEEE) received the B.Sc. degree in electrical and electronics engineering from Eskişehir Osmangazi University, Turkey, in 2006, the M.Sc. degree in electrical engineering from New Mexico Tech, Socorro, NM, USA, in 2008, and the Ph.D. degree in electrical and computer engineering from Texas A&M University, College Station, TX, USA, in 2012. He was a Visiting Research Assistant with the Electrical and Computer Engineering Program, Texas A&M University at Qatar, from 2008 to 2009. In Summer 2012, he was with the Femtocell Interference Management Team, Corporate Research and Development, New Jersey Research Center, Qualcomm Inc. He joined the School of Electrical and Computer Engineering, Oklahoma State University, Stillwater, OK, USA, in 2016, as an Assistant Professor. He has four years of industrial experience at Qualcomm Inc., as a Senior Modem Systems Engineer with the Department of Qualcomm Mobile Computing. His research interests include the design and performance analysis of wireless communications systems in both theoretical and practical point of views, interference modeling, management and optimization in 5G, mmWave, HetNets, cognitive radio systems and applications, satellite communications, visible light sensing, communications and applications, RF channel modeling, non-contact health monitoring, and Internet of Things applications. At Qualcomm Inc., he has received numerous Qualstar Awards for his achievements/contributions on cellular modem receiver design.

ZEESHAN KALEEM received the Ph.D. degree in electronics engineering from INHA University, in 2016. He is currently an Assistant Professor at the Electrical and Computer Engineering Department, COMSATS University Islamabad, Wah Campus. He has published over 50 technical journal and conference papers in reputable venues and also holds 20 U.S. and Korean patents. His current research interests include public safety networks, 5G system testing and development, and unmanned air vehicle (UAV) communications. He received the Research Productivity Award (RPA) from the Pakistan Council of Science and Technology (PSCT), for the year 2016-2017 and 2017-2018. He also received the National HEC Best Innovator Award of the year 2017. He was a co-recipient of the Best Research Proposal Award from SK Telecom, South Korea. He has served/serving as a Guest Editor for Special Issues of the IEEE Access, *Sensors*, the IEEE/KICS Journal of Communications and Networks, and *Physical Communications*, and also served as TPC for world distinguished conferences the IEEE VTC, the IEEE ICC, and the IEEE PIMRC. He is serving as an Associate Technical Editor of prestigious journals/magazine, including the *IEEE Communications Magazine*, the IEEE Access, the IEEE Open Journal of the Communications Society (OJ-COMS), *Computers & Electrical Engineering* (Elsevier), *Human-centric Computing and Information Sciences* (Springer), and *Journal of Information Processing Systems*.

MIROSLAV VOZNAK (Senior Member, IEEE) received the Ph.D. degree in telecommunications from the Faculty of Electrical Engineering and Computer Science, VSB - Technical University of Ostrava, in 2002, and the Habilitation degree, in 2009. He was appointed as a Full Professor in electronics and communications technologies, in 2017. He is the author or coauthor of more than 100 articles in SCI/SCIE journals. His research interests generally focus on information and communication technologies, especially on quality of service and experience, network security, wireless networks, and big data analytics. He has served as a member of editorial boards for several journals, including *Sensors*, *Journal of Communications*, *Elektronika Ir Elektrotechnika*, and *Advances in Electrical and Electronic Engineering*.